

Analysis of the Observation Results for Preferentially Oriented Particles in High-Level Clouds According to the EARLINET Lidar Network and MODIS Data

Alexey Skorokhodov *  and Alexander Konoshonkin

V.E. Zuev Institute of Atmospheric Optics of Siberian Branch of Russian Academy of Sciences,
Academician Zuev Sq. 1, 634055 Tomsk, Russia; sasha_tvo@iao.ru

* Correspondence: vazime@yandex.ru

Abstract: This analysis presents the results of observation episodes for high-level clouds consisting of ice crystals with different orientations in space, using the EARLINET lidar network and MODIS data over Europe from 2015 to 2022. The technique used involves identifying specular reflecting layers through ground-based laser soundings of the atmosphere and finding synchronous images from space, followed by the retrieval of cirrus cloud parameters. The study considers several properties of high-level clouds, including reflection ratio (ρ), effective emissivity (ϵ), optical thickness, effective particle radius, water path, and top height, according to MODIS data. The results of retrieving these properties for cirrus clouds with different orientations of ice crystals over individual EARLINET lidar stations and over Europe as a whole are discussed. The study indicates that high-level clouds with $\rho \geq 0.15$ and $\epsilon \geq 0.4$ definitely contain specular reflecting layers.

Keywords: lidar measurements; high-level clouds; preferentially oriented particles; satellite data; cloud properties



Citation: Skorokhodov, A.; Konoshonkin, A. Analysis of the Observation Results for Preferentially Oriented Particles in High-Level Clouds According to the EARLINET Lidar Network and MODIS Data. *Atmosphere* **2023**, *14*, 1018. <https://doi.org/10.3390/atmos14061018>

Academic Editors: Yoshizumi Kajii and Filomena Romano

Received: 17 April 2023

Revised: 22 May 2023

Accepted: 9 June 2023

Published: 13 June 2023



Copyright: © 2023 by the authors. Licensee MDPI, Basel, Switzerland. This article is an open access article distributed under the terms and conditions of the Creative Commons Attribution (CC BY) license (<https://creativecommons.org/licenses/by/4.0/>).

1. Introduction

High-level clouds (HLCs) are one of the main factors of uncertainty in predicting changes in the Earth's climate [1–3]. On the one hand, cirrus clouds can scatter incoming solar radiation or reflect it back into outer space [4–6], preventing the underlying surface from heating up. On the other hand, HLCs can retain outgoing long-wave radiation in the Earth's troposphere, thereby enhancing the greenhouse effect [7–9]. Considering the high frequency of cirrus clouds, which is 50% at mid-latitudes, and the horizontal extent of their fields, reaching several hundred kilometers, the extent of the existing uncertainty in predicting climate change with an underestimation of the contribution of HLCs becomes clear [10].

According to modern theories, the degree of influence of HLCs on radiative transfer depends on the spatial orientation of the ice crystals of which they are composed [11–13]. If the flat faces of these particles are preferentially oriented in the horizontal plane, then the effect of mirror reflection is observed. With random orientations of the surfaces of ice crystals relative to each other, there is multiple re-reflection (scattering) of the radiation coming to them from space and/or from the underlying surface. The effect of specular reflection of HLCs was first described in [14] using the results of laser polarization sounding. In the presence of layers of ice crystals preferentially oriented in the horizontal plane, strong backscattering and weak depolarization of scattered radiation are observed in cirrus clouds. Later, it was found that the specular reflecting layers in the HLCs can have a vertical extent of several hundred meters, and their lifetime can vary from tens of minutes to several hours [15–17]. In this case, the main reason for the alignment of crystal particles in the horizontal plane is considered to be gravitational settling with a minimal effect of turbulence [18].

The primary method for obtaining information about the spatial orientation of cloud particles is through ground-based lidar systems [19–24]. However, this approach has a significant disadvantage in that it only provides localized measurements, making it impossible to estimate the horizontal dimensions of the specular reflective layers in the HLCs. Recently, attempts have been made to identify features and conditions that facilitate the determination of the spatial orientation of crystal particles in cirrus clouds using data from other remote sensing tools [25].

In [26], an analysis was conducted on the results of retrieving the properties of the HLCs in the Tomsk region (56.46 N, 85.05 E) using the LOZA-M3 lidar [24] and the MODIS spectroradiometer (Aqua and Terra satellites). Cloud parameters that are promising from the perspective of assessing the orientation of ice crystals and retrieved from passive satellite sensing data were identified: reflection ratio ρ and effective emissivity ε . Here, the reflection coefficient refers to the fraction of solar radiation in the visible range reflected by clouds back into outer space [27]. The emissivity shows the proportion of outgoing long-wave radiation retained by the cloud [28]. Additionally, in [26], estimates of their threshold values were obtained in the presence/absence of specular reflecting layers in the HLCs. Thus, at $\rho \geq 0.15$ and $\varepsilon \geq 0.5$, it is assumed that the clouds observed on the MODIS image consist of preferentially oriented ice crystals. The reliability of the threshold values found was confirmed in [29] based on the results of an analysis of active and passive measurements of the HLC properties by the CALIOP lidar (CALIPSO satellite) and the MODIS spectroradiometer, respectively, obtained over Western Siberia from 2006 to 2007, when the lidar off-nadir angle was only 0.3° . It should be noted that the estimates of ρ and ε considered in [26,29] were obtained for a single region of the planet. Therefore, the question of regional features of the properties of specular reflecting layers remains open.

The purpose of this work was to analyze the results of long-term observations of specular reflecting layers in HLCs by the EARLINET (European Aerosol Research Lidar Network) lidar network and the MODIS spectroradiometer, as well as to find the regional features of their properties.

The work is organized as follows. In Section 2, we present the initial data. In Section 3, we present the method for the analysis of ground-based lidar measurements and satellite data. In Section 4, we discuss the obtained results of the comparison of the observations of specular reflecting layers in HLCs. The conclusion and future direction of this study are briefly summarized in Section 5.

2. Materials

The EARLINET lidar network was established in 2000 primarily as a research project to create a comprehensive database of atmospheric and anthropogenic aerosol properties on a continental scale [30]. Currently, EARLINET includes over 30 ground-based laser atmospheric sounding stations located throughout Europe. The database created on the basis of their observational results is one of the main sources of information on the vertical structure of aerosols. The lidars used by EARLINET are not standardized instruments but are constantly being upgraded to improve the quality and quantity of measured parameters. In addition, measurements are not carried out regularly due to weather conditions, equipment maintenance, and more. Therefore, the volumes of information accumulated to date differ by different stations. We used the EARLINET data since 2015, when measurements began to be carried out quite regularly, including the determination of the volume linear depolarization ratio. Data were received from stations in Antikythera (7 episodes), Barcelona (44), Bucharest (33), Warsaw (3), Granada (1), Kuopio (7), Leipzig (58), Lille (29), Limassol (44), Palaiseau (3), Thessaloniki (4), and Évora (49). The geographical coordinates and characteristics of the lidars installed on them can be found in [31]. We have considered the following results of ground-based laser-sounding HLCs by the EARLINET network: their top height (h_{CT}), total attenuated backscatter at a wavelength of 532 nm (β'_{532}), and volume linear depolarization ratio (δ). Moreover, h_{CT} was estimated based on the “cloud-

mask" product if the lidar station provides it or by identifying the highest point with a high value of β'_{532} in the vertical profile.

The results of remote sensing by the MODIS spectroradiometer [32] were used as a source of satellite information. This device is installed on board two satellites, Terra and Aqua, which allows us to obtain 2–4 images over Europe during the daytime between 9:00 and 15:00 UTC. We used the following MODIS data products (Collection 6.1): images in the visible spectrum with a spatial resolution of 1000 m (MOD021KM and MYD021KM), files with reconstructed cloud properties (MOD06_L2 and MYD06_L2), and georeferencing (MOD03 and MYD03). It should be noted that only those episodes of HLC observations were considered when the time between their ground-based and satellite measurements did not exceed 15 min. At the same time, images in the visible range of the spectrum and georeferencing files were used by us to localize the studied fields of cirrus clouds. The products MOD06_L2 and MYD06_L2 served as a source of information about the ratios ρ and ε , as well as the values of optical thickness (τ) (two-channel retrieval using band 2.1 μm), effective particle radius (r_{eff}) (2.1 μm), water path (P) (2.1 μm), and h_{CT} (1 km resolution) [33]. In this case, only those parts of the MODIS images that were obtained at off-nadir angles less than $\pm 40^\circ$ were considered in order to level out the errors in retrieving the above cloud properties [34,35].

3. Method

The main essence of the method for analyzing active ground-based and passive satellite observations of the HLCs is as follows:

(1) Using data from the EARLINET network data, episodes of HLC registration with $h_{CT} > 8000$ m and a vertical extent of less than 1000 m are identified. These threshold values were chosen to exclude convective clouds and mid-level clouds from consideration, which can also consist of crystal particles [36];

(2) Furthermore, the episodes of HLC observation with $\beta'_{532} > 5 \times 10^{-6} \text{ m}^{-1} \cdot \text{sr}^{-1}$ selected at stage 1 are divided into two groups: those containing specular reflecting layers and those consisting of randomly oriented ice crystals. Thus, if $\delta < 0.1$, then cirrus clouds belong to the first group, and when $\delta > 0.4$, they belong to the second group. It should be noted that the threshold values used by us for β'_{532} and δ are stronger than in the original work [37], which is necessary to obtain more reliable analysis results. Figure 1 shows examples of selected episodes of HLC observations over Limassol containing specular reflective layers (11 November 2020 from 12:00 to 12:45 UTC) and consisting of randomly oriented ice crystals (16 March 2022 from 09:45 to 12:00 UTC). In the first case, the cirrus clouds had a vertical extent of about 500 m, and $8800 < h_{CT} \leq 9200$ m, and in the second case, 900 m and $8800 < h_{CT} \leq 10,000$ m, respectively. From Figure 1b, it can be seen that the specular reflecting layer is located in the upper part of the observed cloud. The value of the coefficient δ for cirrus clouds with a random orientation of particles varies from 0.4 to 0.6 according to Figure 1b.

(3) Synchronous MODIS satellite scenes were found for selected episodes of HLC observation with different orientations of crystal particles using known coordinates of lidar stations and georeferencing files MOD03 and MYD03. In this case, only the image on which the studied field of cirrus clouds is closest to the nadir line is selected from all existing images for a specific day. Episodes with a discrepancy of more than 15 min between ground-based lidar measurements and satellite imagery are excluded from consideration. As a result of an analysis of active and passive observations, 132 cases of synchronous registration of specular reflecting layers in the HLCs and 97 episodes of observation of cirrus clouds with a random orientation of particles were selected. Most of these cases were recorded by lidar stations in Barcelona, Bucharest, Leipzig, Limassol, and Évora.

(4) Then, for each episode of synchronous observation of the HLCs with different orientations of crystal particles, the properties τ , r_{eff} , P , ρ , and ε are restored at the points of location of the lidar stations using the products MOD06_L2 and MYD06_L2. The obtained values of the properties of cirrus clouds were used by us to analyze the regional features of

the parameters of the specular reflecting layers, the results of which are presented in the next section.

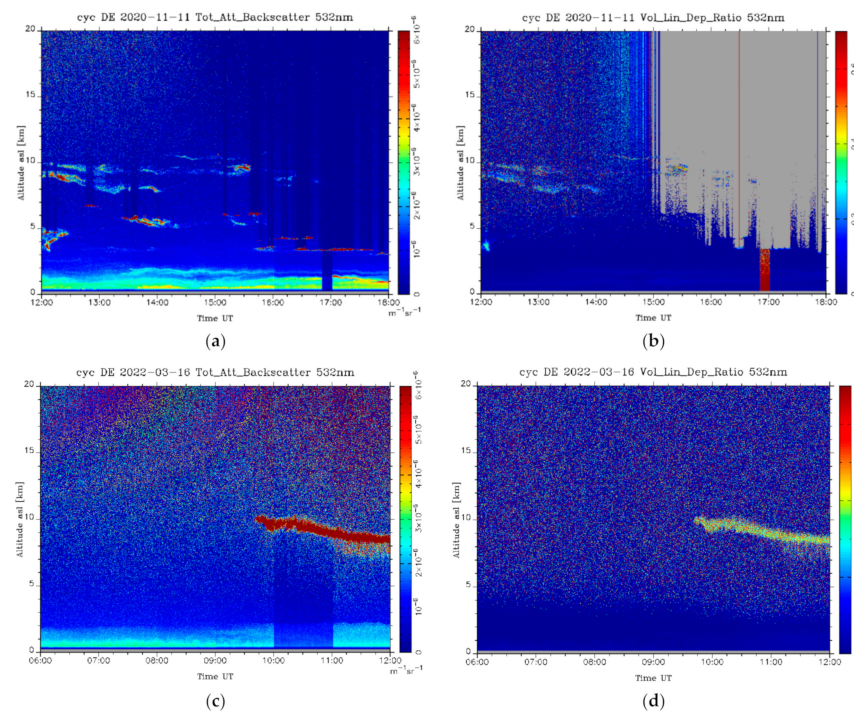


Figure 1. Total attenuated backscatter and volume linear depolarization ratio when observing specular reflective layers in high-level clouds over Limassol (11 November 2020 from 12:00 to 12:45 UTC) (a,b), and cirrus clouds with randomly oriented particles (16 March 2022 from 9:45 to 12:00 UTC) (c) and (d), respectively.

4. Results

Figure 2 shows the scatterplots of the values of ρ and ε for HLCs with different orientations of ice crystals, obtained through long-term synchronous observations by EARLINET lidar stations and the MODIS spectroradiometer. Figure 2 shows that the values $\rho < 0.15$ and $\varepsilon < 0.5$ are typical for the majority of episodes of observation of cirrus clouds with the presence/absence of specular reflecting layers. At $\rho \geq 0.15$ or $\varepsilon \geq 0.5$, the number of cases of observation of HLCs with randomly oriented ice crystals is slightly lower than those with particles preferentially oriented in the horizontal plane. These threshold values are taken from our previous paper [26]. These differences are most pronounced over Barcelona, Leipzig, and Évora. Over Limassol, cirrus clouds with different orientations of ice crystals are practically indistinguishable from each other based on the parameters ρ and ε and generally have low values of these parameters.

Figure 3 shows scatterplots of the values of ρ and ε , ρ and τ , ρ and r_{eff} , and ρ and P for the HLCs with different orientations of crystal particles across all the lidar stations considered in this study. These plots were constructed based on the results of analyzing their data with the long-term MODIS satellite imagery for the period from 2015 to 2022. It can be seen from Figure 3a that at $\rho \geq 0.15$ and $\varepsilon \geq 0.4$, we can confidently speak about the presence of specular reflective layers in cirrus clouds and use these threshold values to detect them from passive satellite sensing data over Europe. The HLC isolated in this case is capable of reflecting more than 15% of solar radiation and retaining more than 40% of the long-wave radiation leaving the underlying surface. The information obtained can be used in solving various scientific and practical problems of climatology and climate modeling related to the study of radiative transfer. At $\rho < 0.15$, cirrus clouds with different orientations of ice crystals are virtually indistinguishable from each other according to passive satellite sounding data. It can be seen from Figure 3b that the specular reflecting

layers can be located in both thin and denser HLCs. At the same time, a region (shown by a dotted line) with a high concentration of episodes of observation of predominantly oriented particles is quite clearly distinguished, compared with randomly oriented with $0.15 \leq \rho \leq 0.25$ and $2 \leq \tau \leq 3.5$. Figure 3c shows that for $\rho < 0.15$, the spread of r_{eff} values is larger than for $\rho \geq 0.15$ and decreases even more with increasing ρ values. At the moment, we cannot explain this feature, which can be considered as a promising direction for the development of this work. It can be seen from Figure 3d that the water path in the HLC, both containing specularly reflecting layers and not containing $\rho \geq 0.15$, is almost the same and varies in the range from 10 to 100 g/m^2 . Moreover, there is an almost identical linear relationship between ρ and P with an almost complete absence of emissions from clouds with different particle orientations, as evidenced by the almost coinciding trend lines in Figure 3d.

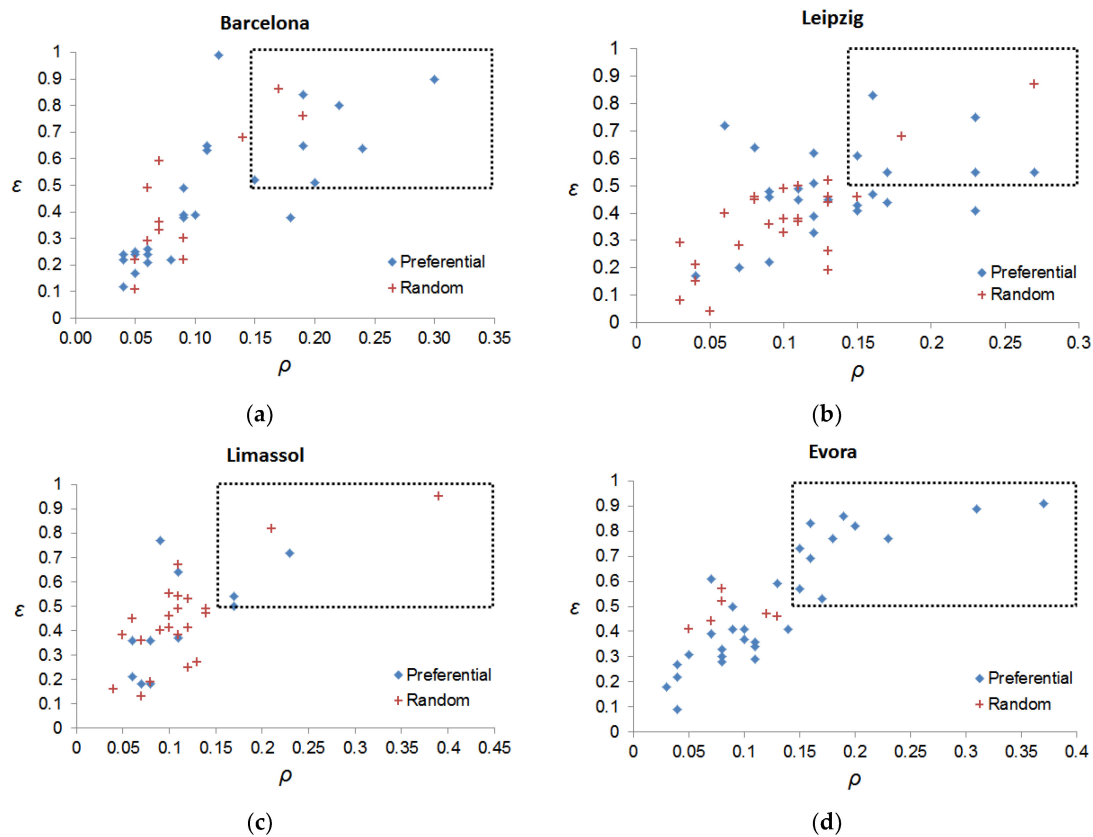


Figure 2. Scatterplots of reflection ratios and effective emissivity for high-level clouds with different orientations of crystal particles, obtained from MODIS data over individual EARLINET lidar stations for the period from 2015 to 2022 for Barcelona (a), Leipzig (b), Limassol (c), and Évora (d).

Table 1 shows the average values of the HLC properties with different ice crystal orientations, retrieved from MODIS satellite data, over individual ground-based lidar stations and across Europe as a whole for the period from 2015 to 2022. Table 1 shows that cirrus clouds with specular reflective layers have higher mean values of reflection coefficients $\langle \rho \rangle$ and effective emissivity $\langle \epsilon \rangle$ than those without. The remaining estimates of the means $\langle \tau \rangle$, $\langle r_{eff} \rangle$, $\langle P \rangle$, and $\langle h_{CT} \rangle$ of the HLCs with different crystal particle orientations are quite similar and demonstrate a different trend over individual lidar stations. We only observed higher values of $\langle h_{CT} \rangle$ for cirrus clouds over Évora, which consists of preferentially oriented ice crystals in the horizontal plane. Overall, and particularly over Limassol, the mean values of the HLC parameters considered in this study with different cloud particle orientations, obtained over various ground-based lidar stations, are quite similar.

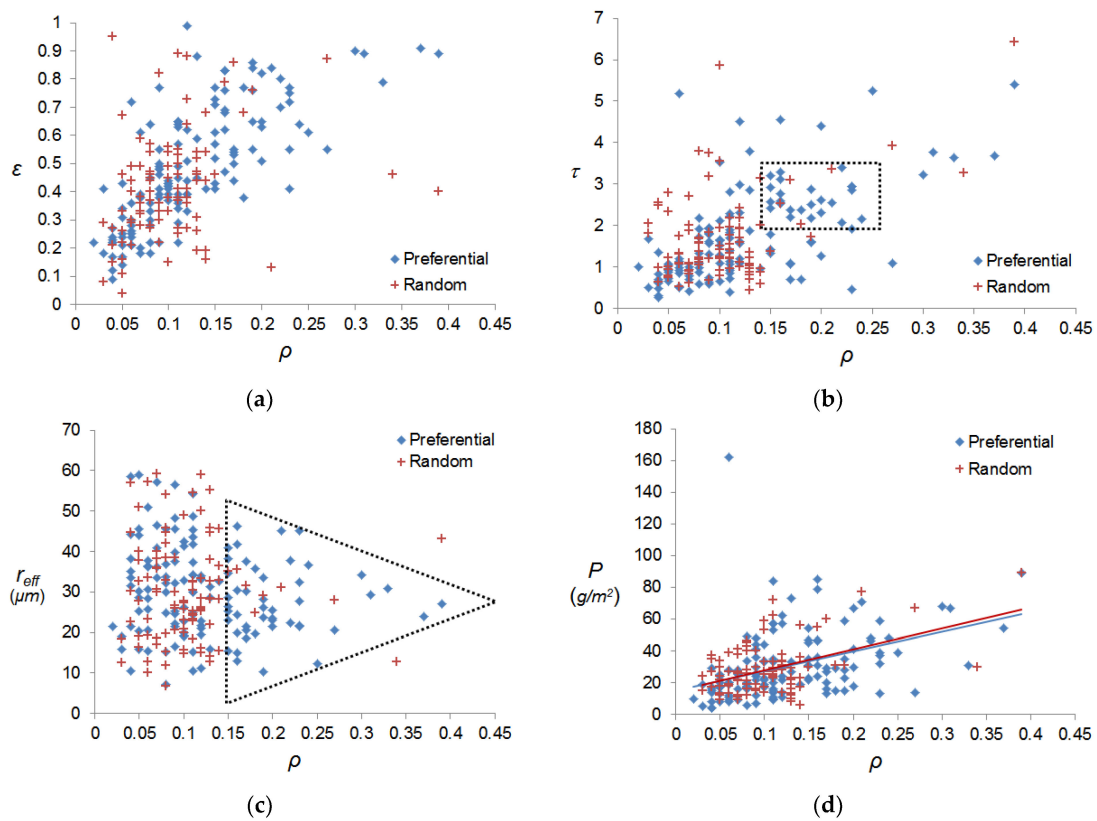


Figure 3. Scatterplots of ρ and ε (a), ρ and τ (b), ρ and r_{eff} (c), and ρ and P (d) for high-level clouds with different orientations of ice crystals obtained from MODIS data over all stations in the EARLINET network for the period from 2015 to 2022.

Table 1. Mean values of the properties of high-level clouds with preferential (P) and random (R) orientation of crystal particles for the period from 2015 to 2022 at various lidar stations in Europe.

Type of Particle Orientation	$\langle \rho \rangle$	$\langle \varepsilon \rangle$	$\langle \tau \rangle$	$\langle r_{eff} \rangle, \mu\text{m}$	$\langle P \rangle, \text{g/m}^2$	$\langle h_{CT} \rangle, \text{m}$
Barcelona						
P	0.12	0.45	1.6	33	30	9800
R	0.09	0.43	1.7	32	32	9300
Leipzig						
P	0.14	0.49	2.0	29	35	10,400
R	0.10	0.38	1.8	30	29	10,100
Lille						
P	0.12	0.44	2.1	27	27	10,400
R	0.11	0.40	1.8	22	22	10,900
Limassol						
P	0.11	0.44	1.5	32	29	10,200
R	0.10	0.42	1.5	34	30	9900
Évora						
P	0.13	0.50	1.6	30	26	10,000
R	0.09	0.48	1.1	37	26	8900
All stations						
P	0.13	0.49	1.8	30	31	10,100
R	0.10	0.43	1.7	31	28	9900

The threshold values ($\rho \geq 0.15$ and $\varepsilon \geq 0.4$) found in this work are consistent with the results of their determination over Western Siberia, as reported in [26]. Therefore, they can be used to estimate the horizontal dimensions of the specular reflecting layers in the HLCs and calculate the mean values of their parameters both on regional and global scales

from long-term satellite data. Figure 4 shows a fragment of the original MODIS image in full size, with the location of the lidar station in Bucharest marked with a red triangle. Figure 4b shows the result of selecting the presumed location of specularly reflecting layers (highlighted in green) among all the HLCs (highlighted in blue). According to the results of laser probing in Figure 4c,d, the specular reflecting layer was located over the entire height of the HLC observation from 11,500 to 15,000 m. The results of retrieving the properties of the cloud field in Figure 4, consisting of preferentially oriented ice crystals, showed that its area is $11,600 \text{ km}^2$, $\langle h_{CT} \rangle = 11,800 \text{ m}$, $\langle \rho \rangle = 0.23$, and $\langle \varepsilon \rangle = 0.71$. Note the homogeneity of the specular reflective layer in Figure 4b, which can have a significant effect on the radiative transfer in the region under study at the considered time point.

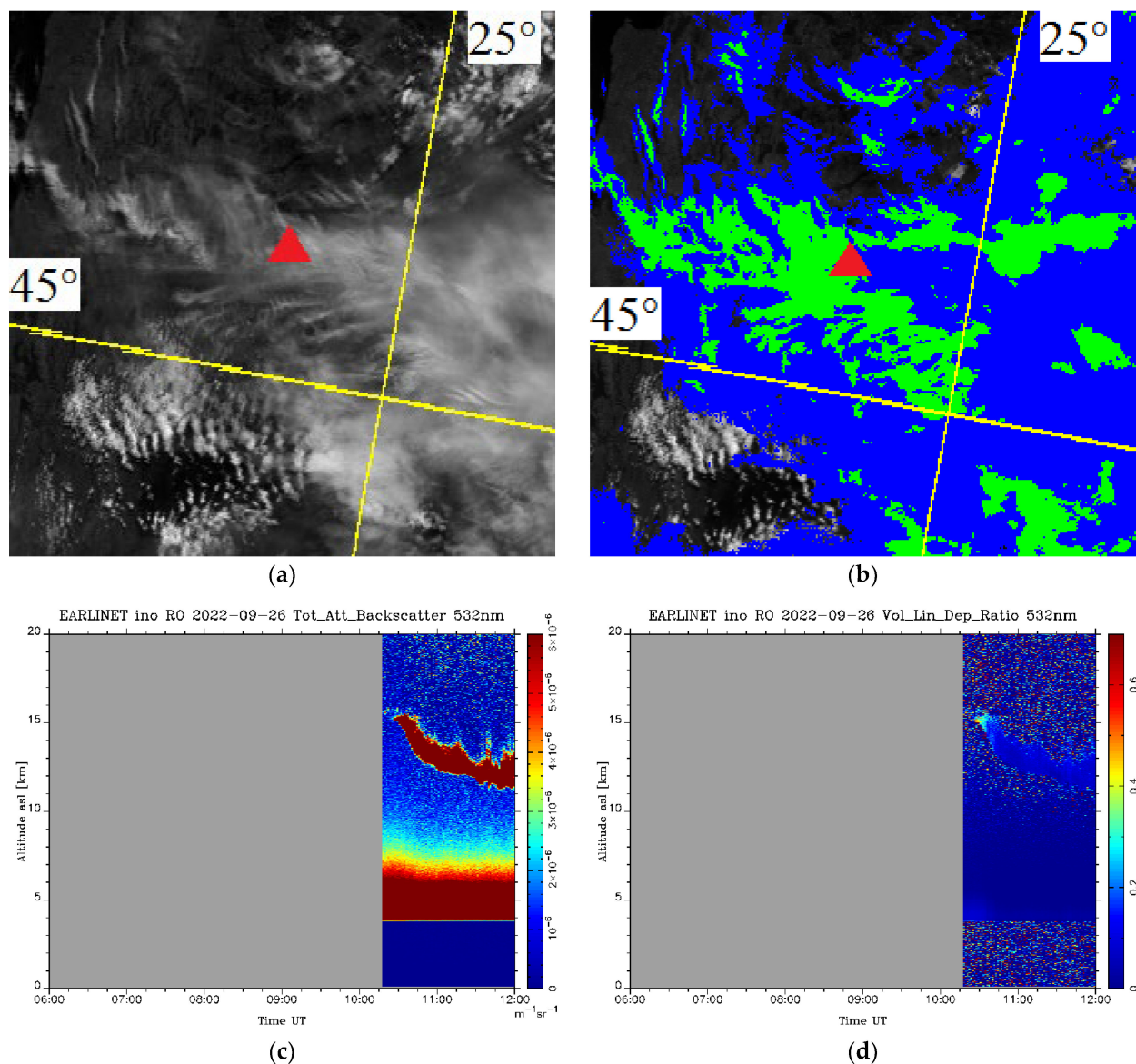


Figure 4. The original MODIS satellite image fragment from 26 September 2022 (11:40 UTC) with the location of the lidar station in Bucharest marked with a red triangle (a). The results of the selection of the presumed location of specular reflective layers (highlighted in green) among all high-level clouds (highlighted in blue) (b), their total attenuated backscatter (c), and the volume linear depolarization ratio (d).

5. Conclusions

This study aimed to identify the characteristic features of specular reflective layers in HLCs by analyzing data from EARLINET ground-based lidar stations and MODIS satellite imagery. Successfully solving this problem would provide ample opportunities to study cirrus clouds, which are composed of ice crystals oriented horizontally, in terms of assessing their impact on radiative transfer in the Earth's atmosphere and predicting future climate change. The results of this study can be considered as a step towards improving the understanding of cloud feedback and its radiative effects. However, before using the threshold values $\rho \geq 0.15$ and $\varepsilon \geq 0.4$ found in this study for operational processing, further research is required. Nonetheless, the results obtained can be used as an auxiliary source of information about the possible sizes of specular-reflecting layers, at least over Europe, in combination with the results of ground-based laser sounding. It is worth noting that the estimates of ρ and ε obtained over Europe are in good agreement with the results given in [26] for Western Siberia. Additionally, the properties of cirrus clouds with different orientations of crystal particles, obtained from MODIS data, are quite similar over different regions of Europe (Figure 1 and Table 1). Furthermore, it was found that specular reflecting layers can be present in both thin HLCs ($\tau < 1$) and in denser ones ($\tau > 5$). In this case, the effective radius of ice crystals oriented horizontally varies from 5 to 60 μm in the region under consideration, and the water path of such cirrus clouds is less than 100 g/m^2 (Figure 3). The threshold values of ρ and ε found in this study can be used to determine the horizontal dimensions of the specular reflecting layers, which are capable of reflecting more than 15% of solar radiation and retaining more than 40% of the outgoing long-wave radiation, in the HLCs over vast areas (Figure 4). A promising area of work is the analysis of the spatial properties of cirrus clouds, consisting of preferentially oriented ice crystals, over various regions of the planet and a comparison of the results obtained on this basis.

Author Contributions: Conceptualization and methodology: A.S. and A.K.; data resources: A.S.; software and validation: A.S.; writing—original draft preparation: A.S.; writing—review and editing: A.K.; funding acquisition: A.K.; supervision and project administration: A.K. All authors have read and agreed to the published version of the manuscript.

Funding: This work was financially supported by the Russian Science Foundation (grant no. 21-77-10089, <https://rscf.ru/project/21-77-10089/>, accessed on 10 April 2023).

Institutional Review Board Statement: Not applicable.

Informed Consent Statement: Not applicable.

Data Availability Statement: Not applicable.

Acknowledgments: Alexander Konoshonkin acknowledges the support of the CAS PIFI (2021VTA0009).

Conflicts of Interest: The authors declare no conflict of interest.

References

1. Lynch, D.K. Cirrus clouds: Their role in climate and global change. *Acta Astronaut.* **1996**, *38*, 859–863. [[CrossRef](#)]
2. Wang, M.; Penner, J.E. Cirrus clouds in a global climate model with a statistical cirrus cloud scheme. *Atmos. Chem. Phys.* **2010**, *10*, 5449–5474. [[CrossRef](#)]
3. Bony, S.; Stevens, B.; Frierson, D.M.W.; Jakob, C.; Kageyama, M.; Pincus, R.; Shepherd, T.G.; Sherwood, S.C.; Siebesma, A.P.; Sobel, A.H.; et al. Clouds, circulation and climate sensitivity. *Nat. Geosci.* **2015**, *8*, 261–268. [[CrossRef](#)]
4. Barja, B.; Antuña-Marrero, J.C. The effect of optically thin cirrus clouds on solar radiation in Camagüey, Cuba. *Atmos. Chem. Phys.* **2011**, *11*, 8625–8634. [[CrossRef](#)]
5. Muri, H.; Kristjánsson, J.E.; Storelvmo, T.; Pfeffer, M.A. The climatic effects of modifying cirrus clouds in a climate engineering framework. *J. Geophys. Res. Atmos.* **2014**, *119*, 4174–4191. [[CrossRef](#)]
6. Zhao, F.; Tang, C.; Dai, C.; Wu, X.; Wei, H. The global distribution of cirrus clouds reflectance based on MODIS Level-3 Data. *Atmosphere* **2020**, *11*, 219. [[CrossRef](#)]
7. Fusina, F.; Spichtinger, P.; Lohmann, U. Impact of ice supersaturated regions and thin cirrus on radiation in the midlatitudes. *J. Geophys. Res.* **2007**, *112*, D24S14. [[CrossRef](#)]
8. Mitchell, D.L.; Finnegan, W. Modification of cirrus clouds to reduce global warming. *Environ. Res. Lett.* **2009**, *4*, 045102. [[CrossRef](#)]

9. Fauchez, T.; Cornet, C.; Szczap, F.; Dubuisson, P.; Rosambert, T. Impact of cirrus clouds heterogeneities on top-of-atmosphere thermal infrared radiation. *Atmos. Chem. Phys.* **2014**, *14*, 5599–5615. [[CrossRef](#)]
10. Matveev, J.L.; Matveev, L.T.; Soldatenko, S.A. *Global Cloud Field*; Gidrometeoizdat: Leningrad, Russia, 1986; pp. 180–184.
11. Baum, B.A.; Yang, P.; Heymsfield, A.J.; Bansemer, A.; Cole, B.H.; Merrelli, A.; Schmitt, C.; Wang, C. Ice cloud single-scattering property models with the full phasematrix at wavelengths from 0.2 to 100 μm . *J. Quant. Spectrosc. Radiat. Transf.* **2014**, *146*, 123–139. [[CrossRef](#)]
12. Konoshonkin, A.; Borovoi, A.; Kustova, N.; Okamoto, H.; Ishimoto, H.; Grynko, Y.; Förstner, J. Light scattering by ice crystals of cirrus clouds: From exact numerical methods to physical-optics approximation. *J. Quant. Spectrosc. Radiat. Transf.* **2017**, *195*, 132–140. [[CrossRef](#)]
13. Stillwell, R.A.; Neely, R.R.; Thayer, J.P.; Walden, V.P.; Shupe, M.D.; Miller, N.B. Radiative influence of horizontally oriented ice crystals over summit, Greenland. *J. Geophys. Res. Atmos.* **2019**, *124*, 12141–12156. [[CrossRef](#)]
14. Platt, C.M.R. Some microphysical properties of an ice cloud from lidar observation of horizontally oriented crystals. *J. Appl. Meteorol.* **1978**, *17*, 1220–1224. [[CrossRef](#)]
15. Giannakaki, E.; Balis, D.S.; Amiridis, V.; Kazadzis, S. Optical and geometrical characteristics of cirrus clouds over a Southern European lidar station. *Atmos. Chem. Phys.* **2007**, *7*, 5519–5530. [[CrossRef](#)]
16. Balin, Y.S.; Kaul, B.V.; Kokhanenko, G.P.; Penner, I.E. Observations of specular reflective particles and layers in crystal clouds. *Opt. Express* **2011**, *19*, 6209–6214. [[CrossRef](#)]
17. Yang, P.; Liou, K.N.; Bi, L.; Liu, C.; Yi, B.; Baum, B.A. On the radiative properties of ice clouds: Light scattering, remote sensing, and radiation parameterization. *Adv. Atmos. Sci.* **2015**, *32*, 32–63. [[CrossRef](#)]
18. Kaul, B.V.; Samokhvalov, I.V. Orientation of particles of Ci crystalline clouds. Part 1. Orientation at gravitational sedimentation. *Opt. Atmos. I Okeana* **2005**, *25*, 963–967.
19. Sassen, K. The polarization lidar technique for cloud research: A review and current assessment. *Bull. Am. Meteorol. Soc.* **1991**, *72*, 1848–1866. [[CrossRef](#)]
20. Liu, Z.; Sugimoto, N.; Murayama, T. Extinction-to-backscatter ratio of Asian dust observed with high-spectral-resolution lidar and Raman lidar. *Appl. Opt.* **2002**, *41*, 2760–2767. [[CrossRef](#)]
21. Neely, R.R.; Hayman, M.; Stillwell, R.A.; Thayer, J.P.; Hardesty, R.M.; O’Neill, M.; Shupe, M.D.; Alvarez, C. Polarization lidar at summit, Greenland for the detection of cloud phase and particle orientation. *J. Atmos. Ocean. Technol.* **2013**, *30*, 1635–1655. [[CrossRef](#)]
22. Ji, C.; Tao, Z.; Hu, S.; Zhang, X.; Liu, D.; Wang, Z.; Zhong, Z.; Xie, X.; Ke’e, Y.; Cao, K.; et al. Effective lidar ratio of cirrus cloud measured by three-wavelength lidar. *Chin. J. Lasers* **2016**, *43*, 0810003.
23. Brown, A.J.; Videen, G.; Zubko, E.; Heavens, N.; Schlegel, N.J.; Beccera, P.; Meyer, C.; Harrison, T.; Hayne, P.; Obbard, R.; et al. The Case for a Multi-Channel Polarization Sensitive LIDAR for Investigation of Insolation-Driven Ices and Atmospheres. Planetary Science Decadal Survey White Paper; ESS Open Archive. 2020. Available online: <https://essopenarchive.org/doi/full/10.1002/essoar.10503720.1> (accessed on 17 March 2023).
24. Kokhanenko, G.P.; Balin, Y.S.; Klemasheva, M.G.; Nasonov, S.V.; Novoselov, M.M.; Penner, I.E.; Samoilova, S.V. Scanning polarization lidar LOSA-M3: Opportunity for research of crystalline particle orientation in the clouds of upper layers. *Atmos. Meas. Tech.* **2020**, *13*, 1113–1127. [[CrossRef](#)]
25. Barlakas, V.; Geer, A.J.; Eriksson, P. *Cloud Particle Orientation and Polarisation for Cross-Track Microwave Sensors in RTTOV*; EUMETSAT Press: Darmstadt, Germany, 2022; pp. 1–20.
26. Skorokhodov, A.V.; Nasonov, S.V.; Konoshonkin, A.V. Comparison of passive satellite data with ground-based lidar observations of specularly reflecting layers in high-level clouds. *Sovrem. Probl. Distantionnogo Zondirovaniya Zemli Iz Kosm.* **2019**, *16*, 263–271. [[CrossRef](#)]
27. Gao, B.-C.; Yang, P.; Han, W.; Li, R.-R.; Wiscombe, W.J. An algorithm using visible and 1.38- μm channels to retrieve cirrus cloud reflectances from aircraft and satellite data. *IEEE Trans. Geosci. Remote Sens.* **2002**, *40*, 1659–1668.
28. Heidinger, A.; Li, Y.; Baum, B.; Holz, R.; Platnick, S.; Yang, P. Retrieval of cirrus cloud optical depth under day and night conditions from MODIS collection 6 cloud property data. *Remote Sens.* **2015**, *7*, 7257–7271. [[CrossRef](#)]
29. Skorokhodov, A.V.; Konoshonkin, A.V. Comparison of satellite active and passive observations of specularly reflecting layers in the high-level clouds. *Sovrem. Probl. Distantionnogo Zondirovaniya Zemli Iz Kosm.* **2021**, *18*, 279–287. [[CrossRef](#)]
30. Bösenberg, J.; Matthias, V. *EARLINET: A European Aerosol Research Lidar Network to Establish an Aerosol Climatology*; MPI-Report 348; Max Planck Institute Press: Hamburg, Germany, 2003; pp. 1–200.
31. EARLINET. Lidar Stations. Available online: <https://www.earlinet.org/index.php?id=105> (accessed on 17 March 2023).
32. LAADS DAAC. Level-1 and Atmosphere Archive & Distribution System Distributed Active Archive Center. Available online: <https://ladsweb.modaps.eosdis.nasa.gov> (accessed on 17 March 2023).
33. Platnick, S.K.; Meyer, G.; King, M.D.; Wind, G.; Amarasinghe, N.; Marchant, B.; Arnold, G.T.; Zhang, Z.; Hubanks, P.A.; Holz, R.E.; et al. The MODIS cloud optical and microphysical products: Collection 6 updates and examples from Terra and Aqua. *IEEE Trans. Geosci. Remote Sens.* **2017**, *55*, 502–525. [[CrossRef](#)]
34. Maddux, B.C.; Ackerman, S.A. Viewing geometry dependencies in MODIS cloud products. *J. Atmos. Ocean. Technol.* **2010**, *27*, 1519–1528. [[CrossRef](#)]

35. Grossvenor, D.P.; Wood, R. The effect of solar zenith angle on MODIS cloud optical and microphysical retrievals within marine liquid water clouds. *Atmos. Chem. Phys.* **2014**, *14*, 7291–7321. [[CrossRef](#)]
36. Zhang, D.; Wang, Z.; Kollias, P.; Vogelmann, A.M.; Yang, K.; Luo, T. Ice particle production in mid-level stratiform mixed-phase clouds observed with collocated A-Train measurements. *Atmos. Chem. Phys.* **2018**, *18*, 4317–4327. [[CrossRef](#)]
37. Sassen, K.; Benson, S. A midlatitude cirrus cloud climatology from the Facility for Atmospheric Remote Sensing: II. Microphysical properties derived from lidar depolarization. *J. Atmos. Sci.* **2001**, *58*, 2103–2112. [[CrossRef](#)]

Disclaimer/Publisher’s Note: The statements, opinions and data contained in all publications are solely those of the individual author(s) and contributor(s) and not of MDPI and/or the editor(s). MDPI and/or the editor(s) disclaim responsibility for any injury to people or property resulting from any ideas, methods, instructions or products referred to in the content.